Scalable and Tunable Carbide-Phosphide Composite Catalyst System for the Thermochemical Conversion of Biomass

Journal:	*ACS Sustainable Chemistry & Engineering*
Manuscript ID	sc-2017-01223t.R1
Manuscript Type:	Article
Date Submitted by the Author:	29-Jun-2017
Complete List of Authors:	Regmi, Yagya; University of Tennessee Institute of Agriculture, Rogers, Bridget; Vanderbilt University, Chemical Engineering Labbe, Nicole; University of Tennessee, Center for Renewable Carbon Chmely, Stephen; University of Tennessee, Center for Renewable Carbon

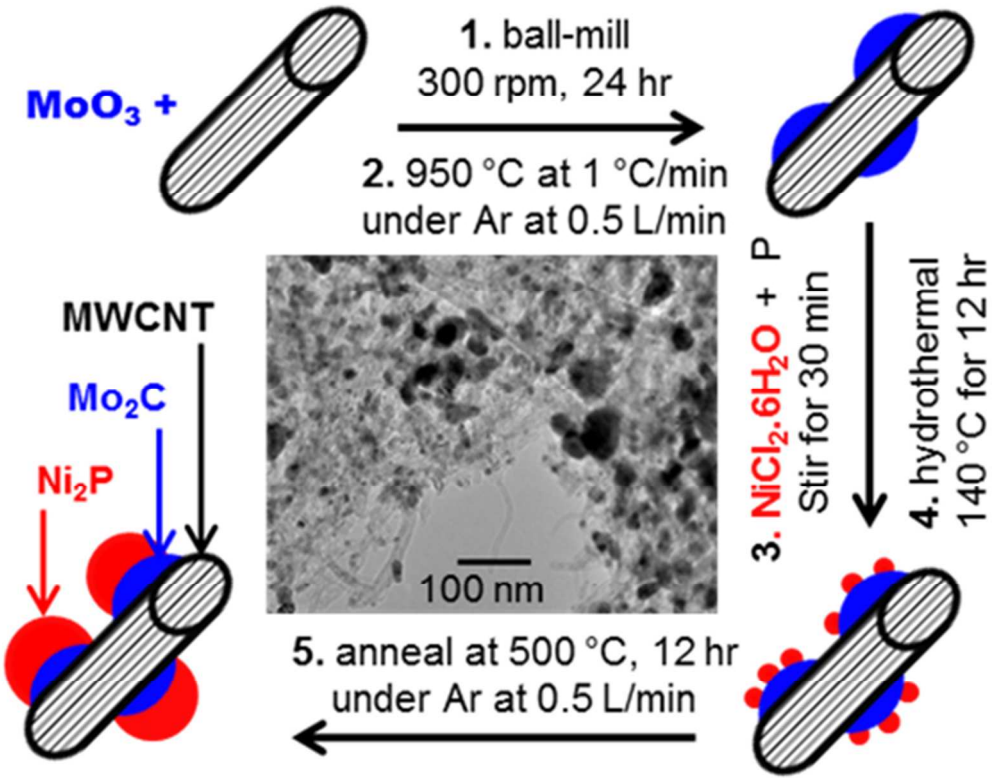

Sequential synthesis scheme for carbide-phosphide composite catalysts. Inset is a TEM micrograph with composite catalysts supported and dispersed on MWCNT.

83x65mm (300 x 300 DPI)

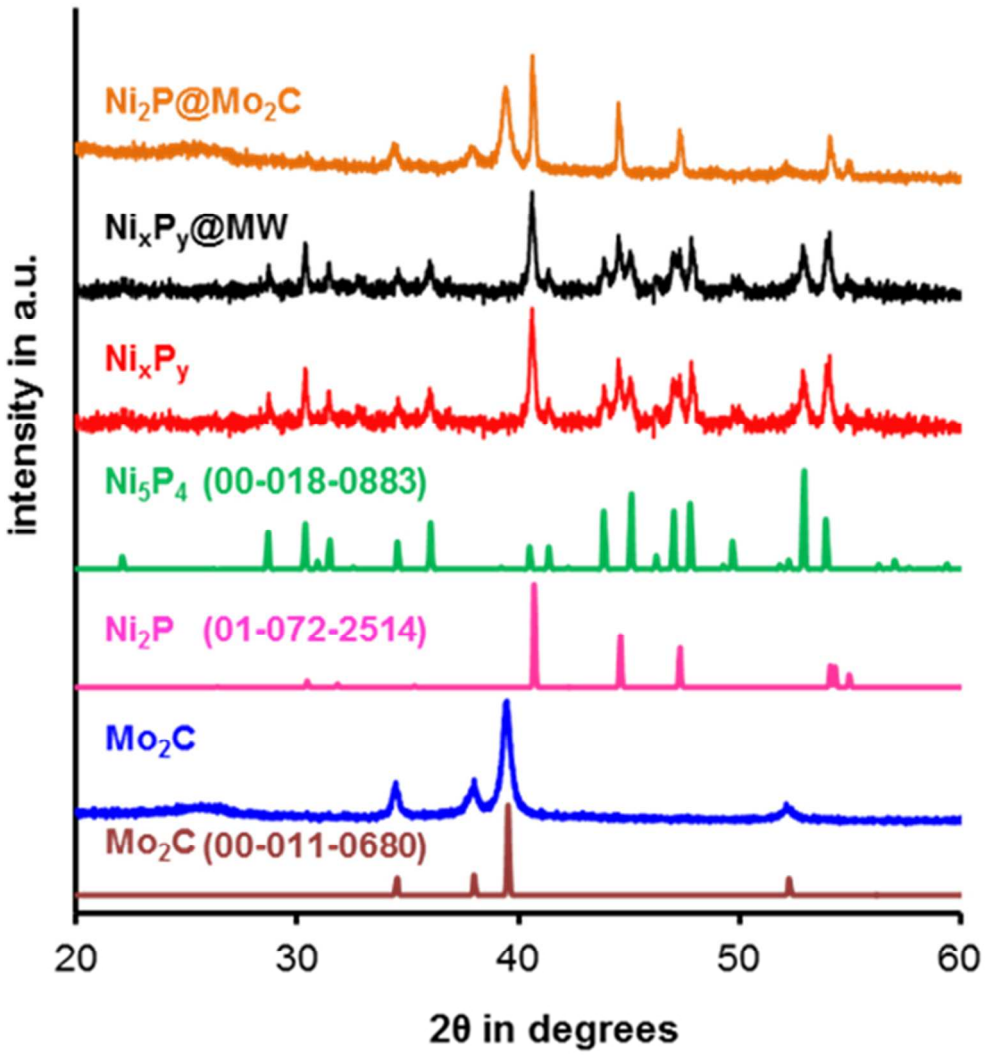

XRD plots of carbide (Mo2C), phosphide (NixPy), the composite catalysts (Ni2P@Mo2C) with molar Ni:Mo = 1.89, and phosphide deposited on MWCNT (NixPy@MW). PDF numbers for reference patterns are listed in parenthesis.

84x88mm (300 x 300 DPI)

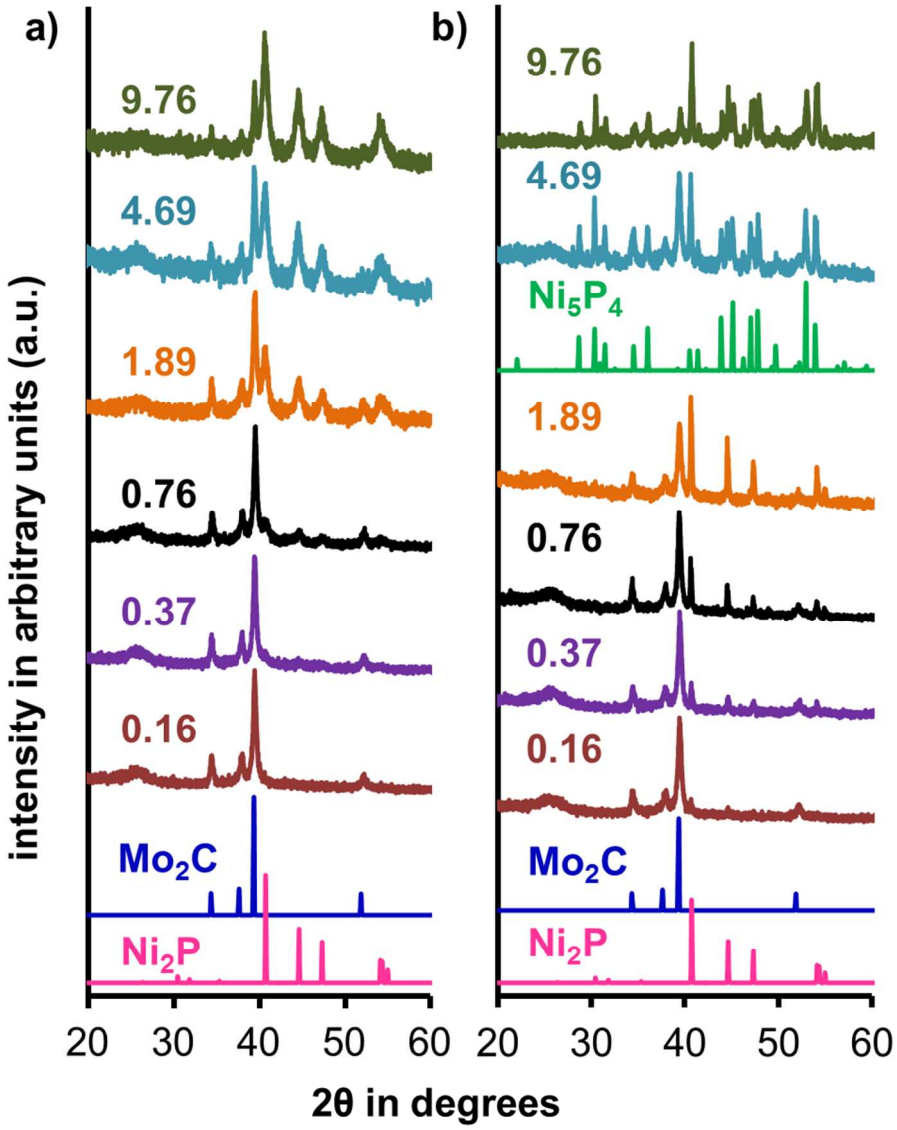

. PXRD diffractograms of (a) as prepared nickel phosphide deposited on molybdenum carbide in the stated molar Ni2P:Mo2C determined via ICP-OES measurements. (b) Phosphide deposited carbides annealed in argon atmosphere at 500 ºC for 12 hours.

84x107mm (300 x 300 DPI)

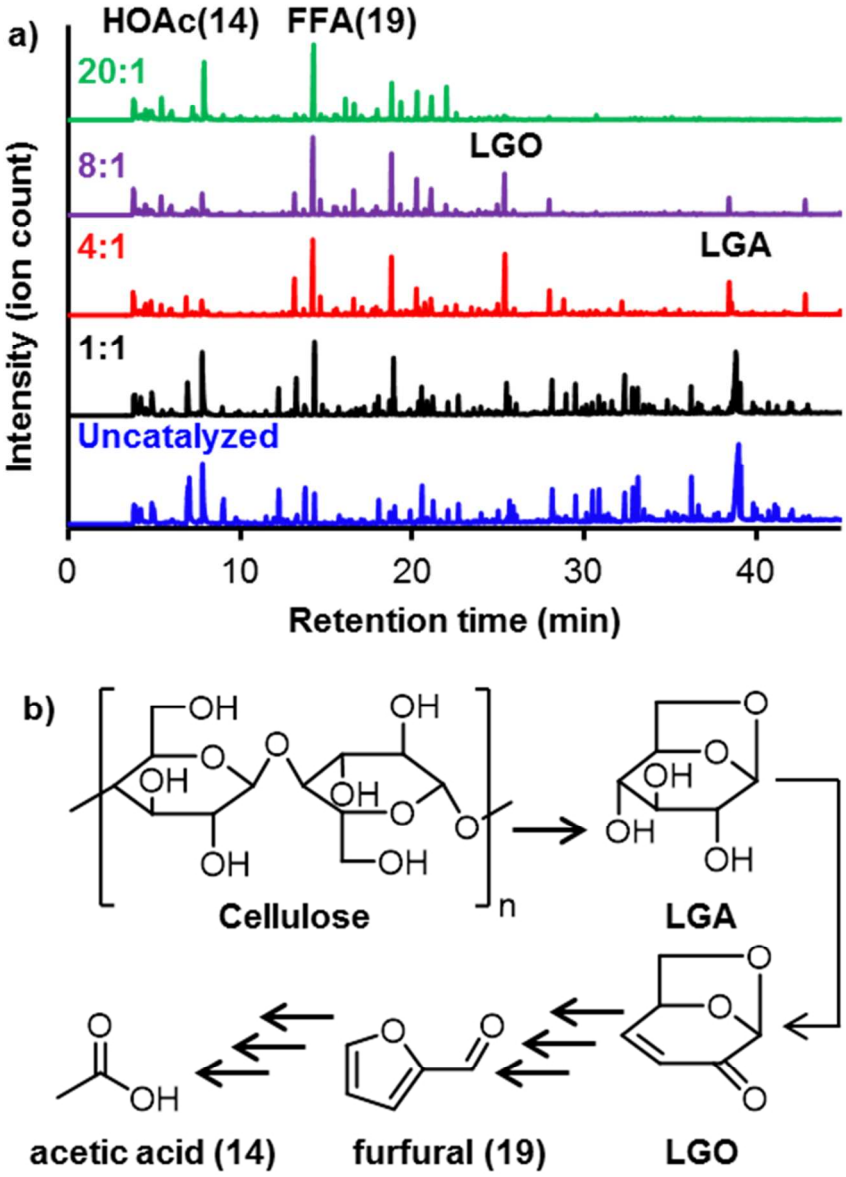

(a) Pyrograms of biomass in the presence of indicated Ni2P@Mo2C catalyst:biomass weight ratios. Peak heights are normalized to the intensity of the tallest peak in each spectrum. (b) Possible reaction pathway for cellulose pyrolysis to levoglucosan and subsequent reaction products.

84x119mm (300 x 300 DPI)

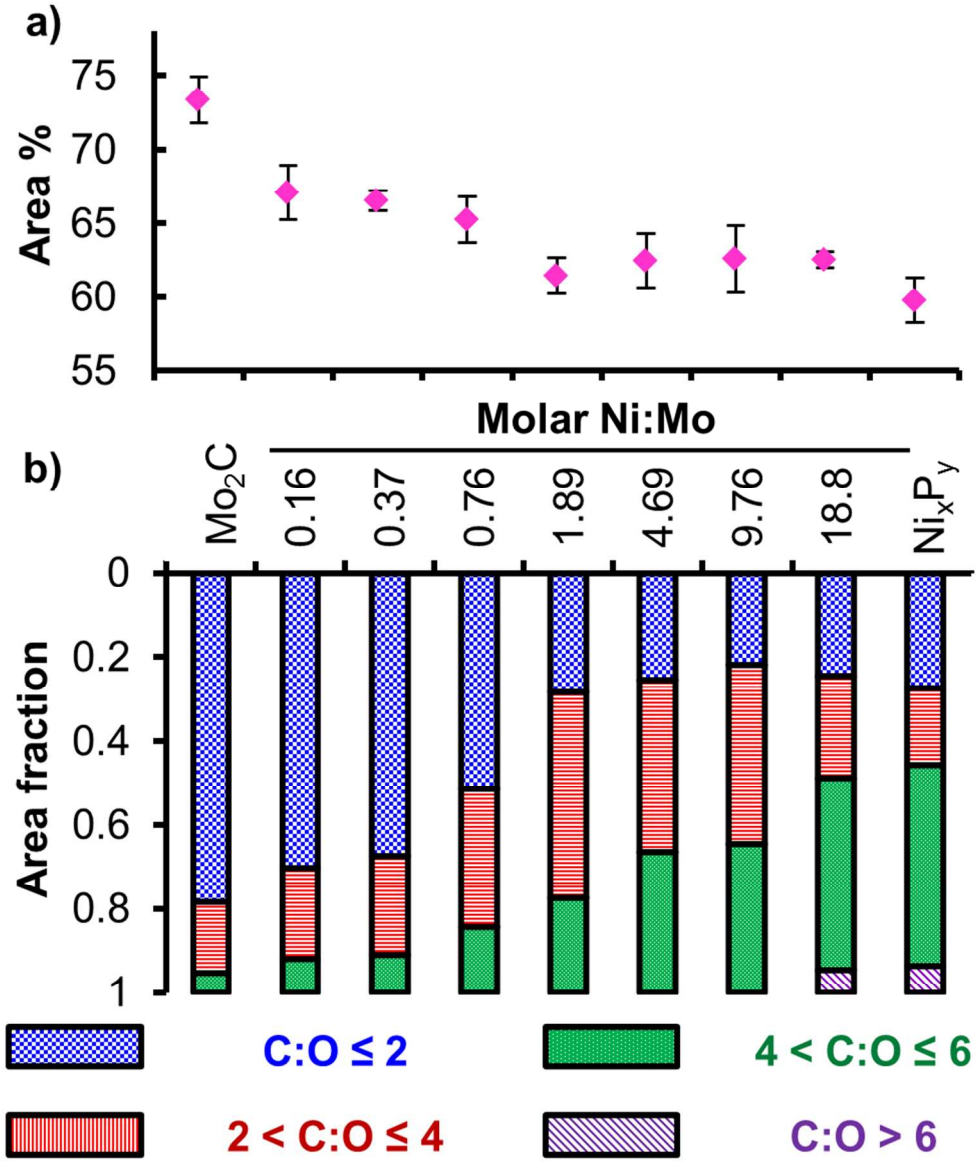

Figure 5: (a) Percent of the total area under the curve represented by the peaks above the threshold (10 % by height) from ex-situ catalytic fast pyrolysis of biomass at 450 °C. (b) Distribution based on carbon to oxygen atomic ratio of products above the threshold.

84x100mm (300 x 300 DPI)

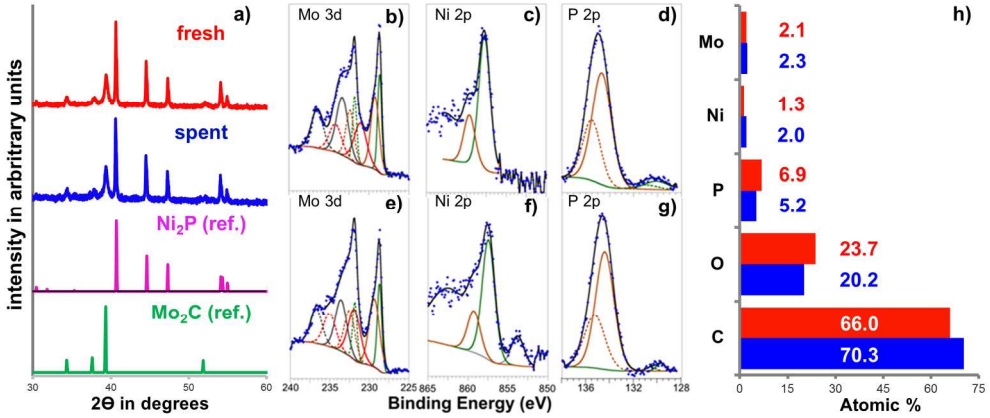

(a) XRD plots for composite phosphide-carbide catalyst before (fresh) and after (spent) biomass upgrading. XPS spectra of Ni2P@Mo2C pre-catalysis corresponding to (b) Mo 3d (c) Ni 2p and (d) P 2p. Post-catalysis XPS spectra corresponding to (e) Mo 3d (f) Ni 2p (g) P 2p. Solid color-coded deconvolution lines in Mo 3d and P 2p spectra correspond to d5/2 and p3/2, respectively. Color matched dotted lines correspond to d3/2 and p½. (h) Bar graph for atomic percent of the fresh (red) and spent (blue) catalyst surfaces determined via XPS.

177x75mm (300 x 300 DPI)

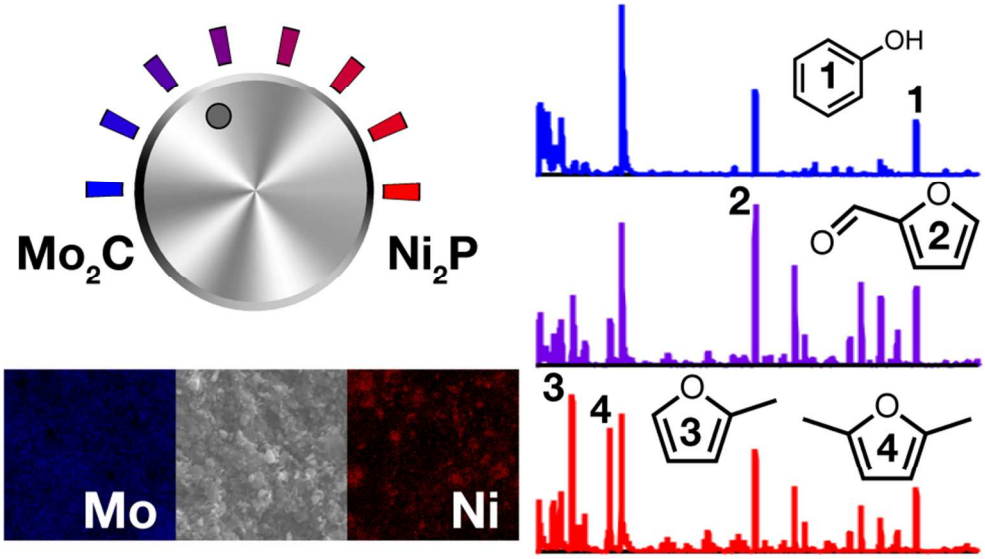

83x47mm (300 x 300 DPI)

Scalable and Tunable Carbide-Phosphide Composite Catalyst System for the Thermochemical Conversion of Biomass

Yagya N. Regmi[ǂ], *B. R. Rogers*[†], *Nicole Labbé*[*,ǂ], *Stephen C. Chmely*[*,ǂ]

ǂ Center for Renewable Carbon, University of Tennessee, 2506 Jacob Drive, Knoxville, Tennessee 37996, United States.

† Chemical and Biomolecular Engineering, 2400 Highland Ave., 107 Olin Hall, Vanderbilt University, Nashville, TN 37235, United States

* nlabbe@utk.edu, schmely@utk.edu

KEYWORDS: Nickel phosphide, molybdenum carbide, vapor phase upgrading, catalytic fast pyrolysis, composite catalysts

ABSTRACT. We have prepared composite materials of hexagonal nickel phosphide and molybdenum carbide (Mo_2C) utilizing a simple and scalable two-stage synthesis method comprised of carbothermic reduction followed by hydrothermal incubation. We observe the monophasic hexagonal phosphide Ni_2P in the composite at low phosphide-to-carbide (P:C) ratios. Upon increasing the proportion of P:C, the carbide surface becomes saturated, and we detect the emergence of a second hexagonal nickel phosphide phase (Ni_5P_4) upon annealing. We demonstrate that vapor-phase upgrading (VPU) of whole biomass via catalytic fast pyrolysis is achievable using the composite material as a catalyst, and we monitor the resulting product slates using pyrolysis gas chromatography/mass spectrometry. Our analysis of the product vapors indicates that variation of the P:C molar ratio in the composite material affords product slates of varying complexity and composition, which is indicated by the number of products and their relative proportions in the product slate. Our results demonstrate that targeted vapor product composition can be obtained, which can potentially be utilized to tune the composition of the bio-oil downstream.

INTRODUCTION

Catalytic fast pyrolysis (CFP) of biomass has tremendous potential to utilize purpose-grown energy crops and agricultural and forest residues as a source of bio-oil.[1,2] Ostensibly, bio-oil could be converted into valuable liquid fuels and products in a manner analogous to petrochemical refining. To accomplish this, however, efficient and stable deoxygenation catalysts for CFP are necessary because of the presence of as much as 40-50% by mass of oxygen in bio-oil, which has been implicated as one source of its instability.[3] Accordingly, transition metal sulfides, nitrides, oxides, carbides, and phosphides have been broadly explored as catalysts for vapor-phase upgrading (VPU) and deoxygenation of pyrolysis vapors.[2,4,5]

That said, transition metal phosphides (TMP) and carbides (TMC) in particular have attracted increased attention as catalysts for biomass valorization because they can mediate an extensive range of transformations, including HDO.[6-9] Among TMPs, hexagonal nickel phosphide (Ni_2P) has been investigated quite frequently and has been synthesized using numerous procedures.[10] Similarly, hexagonal beta-type molybdenum carbide (Mo_2C) is one of the more frequently investigated TMC for biomass upgrading.[11] Mo_2C has been derived using multiple synthesis methods, templated on various carbon structures, and investigated for a range of chemical reactions associated with biomass valorization.[12-14] Moreover, the relatively high earth abundance of Ni and Mo means that catalysts based on them will possess a degree of environmental and economic sustainability not afforded by the use of much rarer noble metals.

Mo_2C has been shown to possess both acidic and basic sites on its surface.[15] The presence of bifunctional and multifunctional sites on a single catalyst surface is particularly advantageous in complex catalytic transformations such as those required for biomass valorization, where

multiple reactions involving myriad analytes varying in molecular weight and complexity proceed simultaneously. Accordingly, Bhan and coworkers have demonstrated that specific sites on Mo_2C can be selectively deactivated, which provides additional control over the catalytic behavior of these materials.[16] The same group also demonstrated high selectivity for deoxygenated aromatic products when a mixture of lignin derived phenolic compounds was subjected to HDO over an Mo_2C surface.[17]

Our own recent investigation of these materials led us to produce various Ni_2P@Mo_2C composites that are capable of mediating the hydrogen evolution reaction (HER).[18] Those experiments demonstrated the utility of the phosphide-carbide interaction to the long-term stability of the catalyst. Similarly, the groups of Jensen[19] and Heeres[20] have demonstrated that metal-support interaction is crucial to maintain the activity and stability of hydrotreating catalysts based on Ni and Ni-Cu bimetallics. Moreover, research carried out by Oyama[21] and Lin[22] has demonstrated the utility of supported nickel phosphide catalysts for the deoxygenation of bio-oil and lignin model compounds, respectively. Given the elegant studies involving HDO of biomass and related compounds using nickel phosphide and molybdenum carbide, we were intrigued by the possibility of using our composite material for biomass valorization via CFP.

Herein we report structural properties of a family of Ni_2P@Mo_2C composite materials that contain various ratios of phosphide to carbide (P:C). We have employed these materials in CFP of *Populus deltoidies* (hybrid poplar) hybrid crosses. We monitored the major products of CFP using pyrolysis-gas chromatography/mass spectrometry (py-GC/MS) and investigated the effect of catalyst mass ratio and composition on the resulting vapor products. We propose that lattice matching and the common hexagonal crystal structure of Ni_2P and Mo_2C is responsible for carbide-phosphide composite formation. We also postulate that interfacial areas of phosphide

and carbide result in unique bimetallic active sites. The presence of these sites affords the ability to tune the product slate of CFP by modulating the P:C ratio in the catalyst. Finally, we compare catalyst properties before and after catalysis using X-ray photoelectron spectroscopy (XPS), powder X-ray diffraction (PXRD) and energy dispersive X-ray spectroscopy (EDS) to demonstrate variations in catalyst composition and overall catalyst stability.

EXPERIMENTAL SECTION

Materials

MoO_3, multi-walled carbon nanotubes (MWCNT), red phosphorus, and $NiCl_2.6H_2O$ were purchased from Sigma-Aldrich. Anhydrous ethanol, methanol, acetone, and concentrated nitric and hydrochloric acids were purchased from Fisher Scientific. Hydrofluoric acid, boric acid and naphthalene (99 %) were purchased from Acros Organics. Stock solutions for inductively coupled plasma optical emission spectroscopy (ICP-OES) of Ni (20 ppm), Mo (1000 ppm) and P (1000 ppm) were purchased from SPEX CertiPrep. All the materials were used as received unless otherwise stated. Biomass **(**hybrid poplar**),** organosolv fractionation derived lignin and cellulose were obtained from the Center for Renewable Carbon (The University of Tennessee).

Catalyst synthesis

Carbide synthesis was modified from the carbothermic reduction method reported previously.[23] Briefly, a mass ratio of 20:1 ball to precursor mixture of MoO_3 and MWCNT was ball-milled at 300 rpm for 20 hours. The resulting mixture was heated in a 1" tube furnace to 950 ºC using a ramp rate of 1 ºC/min under argon flow at 0.5 L/min. Without any dwelling, the furnace was cooled to the ambient temperature and the resulting powder was ground using an

agate mortar and pestle. Ni_2P and $Ni_2P@Mo_2C$ catalysts with various Ni:Mo molar ratios were synthesized by adopting the method described by Deng et al and described in detail in our recent report.[18,24] For example, to obtain the catalyst with Ni:Mo = 1.89, 30 mL of an aqueous solution of $NiCl_2.6H_2O$ (0.95 g, 4.0 mmol) was stirred at 400 rpm for 10 min. Then, elemental red phosphorus (0.70 g, 23.0 mmol) was added, followed by as-prepared Mo_2C (0.41 g, 37 wt% Mo). The resulting mixture was stirred for 20 min. Then, the slurry was transferred into a Teflon lined hydrothermal bomb from Parr Instruments and incubated at 140 ºC for 12 hours. After cooling to room temperature, the black suspension was washed via centrifugation (3500 x g) with three 50 mL portions of DI water and one portion of anhydrous ethanol. The residue was dried at 60 ºC under vacuum for 6 h. The resulting powders were ground with a mortar and pestle and annealed in a 1" tube furnace under argon flow at 500 ºC for 12 h to remove excess phosphorus. Synthesis of Ni_2P was identical except for the absence of Mo_2C. $Ni_2P@MW$ was also prepared by replacing Mo_2C with MWCNT, and a physical mixture of Ni_2P and Mo_2C was obtained by grinding of as-prepared Mo_2C (0.41 g) and Ni_2P (0.30 g) for 20 min.

Characterization

PXRD was conducted on a Pananalytical Empyrean diffractometer with Cu K alpha1 source (λ = 1.5406 Å). Instrumental broadening for Scherrer Analysis for background corrections were based on diffraction pattern of LaB_6 standard (660) purchased from the National Institute of Standards and Technology (NIST). The reference patterns were obtained from PDF-4 database from International Center for Diffraction Data (ICDD). Thermogravimetric analysis (TGA) studies were conducted on a TA Discovery Series thermogravimetric analyzer with N_2 (0.100 L/min) as the carrier gas. Scanning electron micrographs and EDS maps were generated on a Zeiss EVO instrument equipped with EDS detector from Bruker. Transmission electron

microscopy (TEM) was performed on a Zeiss Libra 200 HT FE MC instrument and TEM-EDS on a FEI Tecnai Osiris™ 200 kV scanning TEM equipped with EDS. The samples were supported on copper grids with formvar film on 400 square mesh. XPS analyses were performed using an Ulvac-PHI Versaprobe 5000. Monochromatic Al Kα X-rays (1486 eV), a 100 μm diameter X-ray spot, and a takeoff angle of 60 degrees off sample normal were used in each acquisition. Pass energies for the survey and high-resolution acquisitions were 187.7 eV and 23.5 eV, respectively. Charge neutralization was attained using 1.1 eV electrons and 10 eV Ar+ ions. The powder samples were pressed into a piece of indium foil and the foil was screwed onto a sample puck. Minor energy shifts due to charging were corrected by placing the -CH_2- type bonding in the carbon 1s spectrum at 284.8 eV. Calculated peak areas and sensitivity factors from PHI handbook were used to determine the relative atomic concentrations.[25] ICP-OES measurements were performed on an Optima 7300 DV spectrometer from PerkinElmer after digestion of the catalysts using a previously described microwave assisted method.[26]

Catalytic fast pyrolysis of biomass

Pyrolysis of biomass and analysis of the resultant vapor were performed on a PerkinElmer Clarus 680 gas chromatograph (GC) connected to a Clarus SQ 8C mass spectrometer (MS). The GC-MS assembly was equipped with a Frontier EGA/Py-3030 D pyrolyzer and autosampler. The details of pyrolysis method and analysis of the data have been described previously.[27] Briefly, samples were prepared by alternating layers of 0.500 mg biomass, 1 mg washed quartz wool, a prescribed amount of catalyst, and a final layer of 1 mg washed quartz wool in stainless steel autosampler cups (d = 4 mm, h = 8 mm). Naphthalene (50 μg) was added in the biomass layer as the internal standard (I.S.) for semi-quantitation experiments. The as-prepared cups were pyrolyzed at 450 °C for 12 s, and the resulting vapor was introduced into the GC in a split ratio

of 80:1. The unpacked 2 mm quartz liner injector port was maintained at 280 °C and the ultra-high purity helium (99.9999%) was the carrier gas. The GC column (Agilent DB-1701) pressure was maintained at 17.3 psi and the flow rate at 1 cm^3/min. The column temperature was held at 50 °C for 4 min followed by ramping to 280 °C at 5 °C/min, and finally held at 280 C for 4 min. The GC fractions were analyzed using MS with source temperature and ionization voltage at 280 °C and 70 eV, respectively. Compounds were identified by in-house prepared retention time library and/or comparing the fragmentation patterns with the National Institute of Standards and Technology (NIST) database. Each experiment was repeated at least four times for reproducibility and error calculations. Spent catalysts from five py-GC/MS replicates catalyzed by Ni_2P@Mo_2C(1.89) at 20:1 catalyst to biomass ratio were combined for XPS and XRD studies. The spent catalyst includes the quartz wool and post-pyrolysis carbonaceous material.

RESULTS AND DISCUSSION

Catalyst synthesis and characterization

A sequential synthesis scheme, comprising of carbothermic reduction of molybdenum oxide with MWCNT followed by hydrothermal deposition of phosphide on as synthesized carbide, was utilized to prepare carbide-phosphide composite catalysts. Carbothermic reduction and hydrothermal synthesis methods were selected because of their potential towards scaled up synthesis. Catalyst yield is easily scaled by adjusting the tube furnace size for carbothermic reduction and incubator size for hydrothermal synthesis. As illustrated in Figure 1, the precursor mixture of oxide and MWCNT was ball-milled prior to carbothermic reduction to obtain homogenous mixture and thus improve dispersity of carbide nanoparticles in carbon nanotube matrix (Figure S1a and S1d).

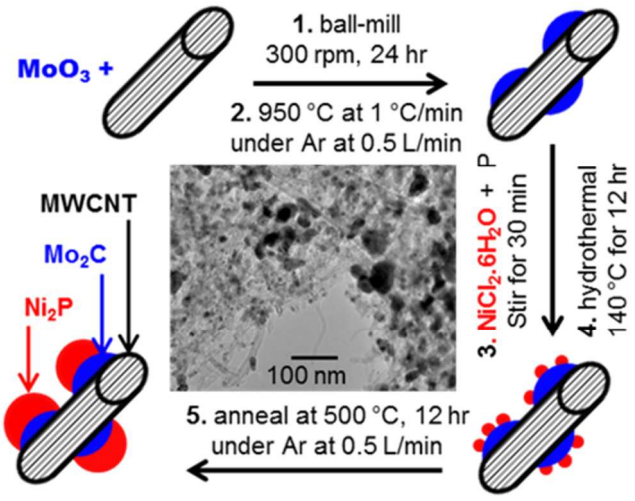

Figure 1. Sequential synthesis scheme for carbide-phosphide composite catalysts. Inset is a TEM micrograph with composite catalysts supported and dispersed on MWCNT.

Unsupported nickel phosphide (Ni_xP_y) was synthesized in the absence of any substrate (Figure S1b and S1e) while phosphide supported on MWCNT (Ni_xP_y@MW) was prepared by adding MWCNT instead of carbide. Zhao has recently reported that under hydrothermal conditions and metal chlorides as precursors, phosphide formation propagates via the formation of metal hydroxide and elemental metal prior to phosphidation.[28] Also, since Mo_2C remains unaffected under hydrothermal conditions as reported by Tang et al.,[29] we infer that formation of the phosphide proceeds via an analogous route in the presence of carbide. Phosphide nanoparticles were thus formed in-situ and hydrothermally deposited onto the carbide matrix at 140 °C (Figure S1c and S1f). Hydrothermal synthesis of nickel phosphide requires a large molar excess of phosphorus (P:Ni = 5.7), the presence of which could be detrimental to catalytic reactivity. Given previous reports regarding the sublimation range of red P between 380-525 °C, we have determined by TGA that excess elemental P is conveniently removed by annealing at 500 °C under argon (Figure S2).[30,31]

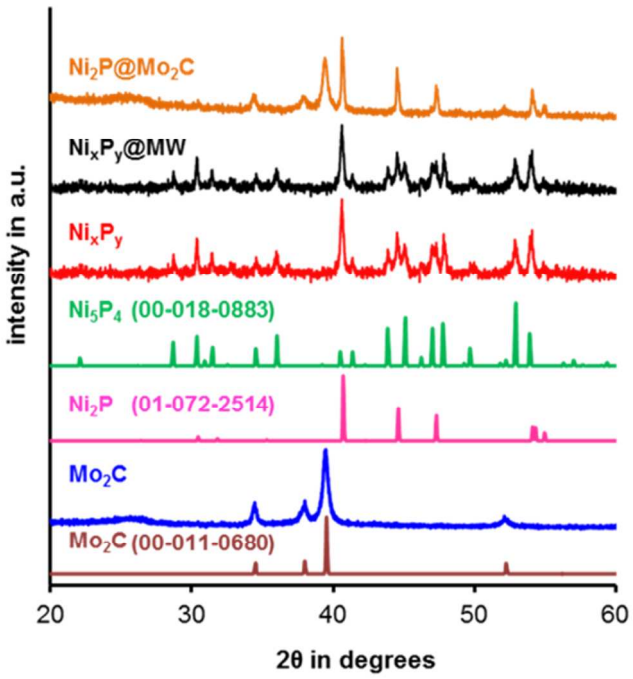

Figure 2. XRD plots of carbide (Mo_2C), phosphide (Ni_xP_y), the composite catalysts ($Ni_2P@Mo_2C$) with molar Ni:Mo = 1.89, and phosphide deposited on MWCNT ($Ni_xP_y@MW$). PDF numbers for reference patterns are listed in parenthesis.

Powder X-ray diffraction (PXRD) patterns of the annealed composite materials and references are shown in Figure 2. Carbothermic reduction of MoO_3 with MWCNT as the source of carbon results in phase pure hexagonal β-Mo_2C (blue). Both unsupported (red) and MWCNT-supported (black) nickel phosphide form a biphasic mixture of two hexagonal phosphides, Ni_2P and Ni_5P_4. The PXRD pattern of the composite material (orange) contains peaks corresponding to only Mo_2C and Ni_2P. Peaks corresponding to the Ni_5P_4 phosphide phase are absent in the composite material. The hexagonal crystal structure of molybdenum carbide remains unchanged under the hydrothermal conditions utilized during the synthesis, as apparent from the diffraction pattern for $Ni_2P@Mo_2C$ (orange), which agrees with earlier observations reported for the synthesis of molybdenum sulfide-carbide composite material.[29] Peaks corresponding to

molybdenum oxides, molybdenum phosphide and NiMo bimetallic alloys or compounds are also not observed. The broad peak around 25° 2θ for Mo_2C and $Ni_2P@Mo_2C$ corresponds to graphitic carbon 002 peak from MWCNT.[32]

Figure 3 reveals the effects of Ni:Mo ratio and annealing temperature on the composition of the resulting materials. All as-synthesized $Ni_2P@Mo_2C$ composites consist of a monophasic phosphide deposited on carbide (Figure 3a). However, when the materials are annealed at 500 °C under flowing argon, Ni_2P is the only detected phosphide phase until the Ni:Mo molar ratio exceeds 1.89. At higher ratios, two phosphide phases are observed (Figure 3b). As apparent in Figure 2, annealing unsupported nickel phosphide (red) and MWCNT-supported phosphide (black) affords a biphasic mixture as well. Apparently, the carbide surface is saturated with phosphide at around 1.89 Ni:Mo molar ratio. At higher phosphide loading, any additional hydrothermally prepared nickel phosphide is either not in direct contact with the carbide surface or it is depositing on MWCNT. Evidently, a direct interaction between the phosphide and carbide surfaces is critical to retain a monophasic nickel phosphide under annealing conditions employed during the current investigation. The hydrothermal conditions were selected to preclude any other phosphide phases except Ni_2P in as prepared composites.[24] As noted by our group and others, Ni_2P and Ni_5P_4 phases seem to exist in a dynamic equilibrium with the equilibrium temperature around 350 °C.[18,33] The carbide-phosphide interaction perhaps shifts the equilibrium towards Ni_2P phase over Ni_5P_4 at higher temperatures.

As apparent from Figure S1a, there is ubiquitous bare carbon surface from MWCNT instead of carbide in the Mo_2C matrix for the phosphide to be deposited. The apparent preference of phosphide to deposit on carbide instead of carbon can perhaps be attributed to the presence of acid and base sites on Mo_2C surface.[15,16,34] The presence of multifunctional sites on carbide

surface may be facilitating the deposition of intermediate species such as nickel hydroxides and nickel on carbide instead of carbon, and ultimately the formation of phosphide on Mo_2C.[28]

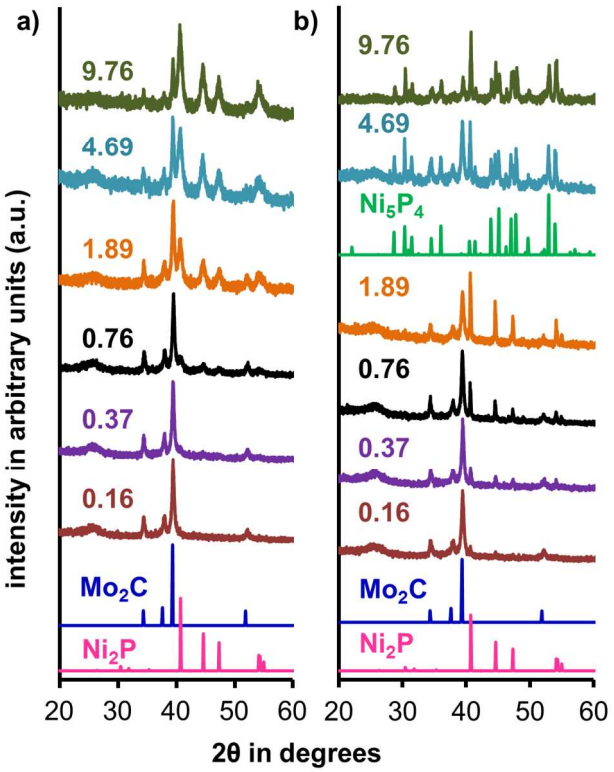

Figure 3. PXRD diffractograms of (a) as prepared nickel phosphide deposited on molybdenum carbide in the stated molar Ni_2P:Mo_2C determined via ICP-OES measurements. (b) Phosphide deposited carbides annealed in argon atmosphere at 500 ºC for 12 hours.

The carbide-phosphide composite formation can also additionally be attributed to the low degree of lattice mismatch between several pairs of low angle lattice planes from the two materials. As shown in Table 1, three out of the first four low-angle lattice planes from Mo_2C are within 3 % mismatch to a prominent low angle lattice planes in Ni_2P. The only exception is 002 from Mo_2C that does not have a corresponding plane in Ni_2P within five percent mismatch.

Significantly, the most prominent lattice plane of Ni_2P, 111, shows only 2.681 % mismatch with the most prominent counterpart in Mo_2C, the 011 plane.

Table 1. Lattice mismatch of first four low angle diffraction peaks for Mo_2C (PDF: 00-011-0680) with corresponding D-spacing and diffractions peaks of Ni_2P (PDF: 01-072-2514).

Mo_2C		Ni_2P		Mismatch (%)
hkl	D (Å)	hkl	D (Å)	
010	2.595	020	2.537	2.235
002	2.364	111	2.214	6.345
011	2.275	111	2.214	2.681
012	1.748	030	1.692	3.204

Analysis of the PXRD plots in Figures 2 and 3 show that the carbide crystallite size does not change significantly during the hydrothermal incubation or annealing. Scherrer analysis of the XRD peak shows that the crystallite size of molybdenum carbide is approximately 18 nm before (Figure 3a) and 23 nm after (Figure 3b) annealing. Thus, Mo_2C is a stable catalyst support and remains structurally and compositionally unaffected during the synthesis and subsequent annealing procedures employed here. However, the nickel phosphide crystallite average size increases from 11 nm to 49 nm upon annealing, as apparent from Figure 3 and Scherrer analysis.

As we have shown in a recent report, X-ray photoelectron spectroscopy (XPS) analysis of the catalyst surfaces reveals that the carbide-phosphide composite material is substantially different from the individual carbide and phosphide materials.[18] We noted a shift to higher binding energies for Mo $3d_{5/2}$ in the composite material as compared to monophasic Mo_2C. Li and Zhao recently reported an increase of 0.33 eV when Fe was doped into Ni compounds.[35] Similarly,

Abu and Smith had reported shifts to higher binding energies when Co was doped into Ni_2P and MoP.[36] Thus, we concluded that the higher binding energy shift (~ 0.50 eV) for Mo 3d peaks are the result of an intermetallic interaction between Mo and Ni in the composite material.

Catalytic fast pyrolysis (CFP) of biomass

We have employed py-GC/MS to investigate the effect of catalyst on the composition of the product slate from CFP of hybrid poplar. We initially selected a low catalyst loading (1:1 catalyst:analyte) to retain complexity in terms of the number of products detected in the vapor product post-CFP. The product slate from CFP is significantly different from uncatalyzed VPU, as apparent from the differences in corresponding pyrograms (Figure S3). The most prominent difference between Mo_2C- and Ni_xP_y-catalyzed systems is the ratio of levoglucosan (LGA) to levoglucosenone (LGO): the carbide system affords more LGA while the phosphide system affords more LGO. The product slate afforded by the composite material ($Ni_2P@Mo_2C$) is subtly different when compared to that afforded by a carbide-phosphide physical mixture. Close inspection of the related pyrograms reveals those differences between the relative peak heights.

As shown in Figure 4a, increasing the catalyst to analyte ratio from 1:1 to 20:1 decreases the number of prominent compounds at higher RT (> 22 min) in the product slate. A decrease in the intensity of the peaks corresponding to primary cellulose, hemicellulose and lignin pyrolysis products is evident at higher catalyst loading, which indicates more of the primary product vapor compounds contacted the catalyst active sites. Huber and co-workers have proposed that under CFP conditions, the depolymerization of cellulose affords glucose, which undergoes a dehydration to form LGA.[37] Further dehydration of LGA affords LGO, as apparent from Figure 4b, representing a pathway for deconstruction of the cellulosic portion of biomass.[38] At higher

catalyst loading (up to 4:1), a decrease in LGA and an increase in LGO peak intensities indicates the utility of the catalyst material for mediating these dehydration reactions. At the highest loading investigated here (catalyst:biomass = 20:1), LGA and LGO are all but completely consumed, and acetic acid and furfural dominate the product slate. Formation of furfural and subsequent products such as acetic acid and CO_2 from LGO has been proposed to proceed through a complex series of dehydration, decarbonylation and decarboxylation reactions.[37-39]

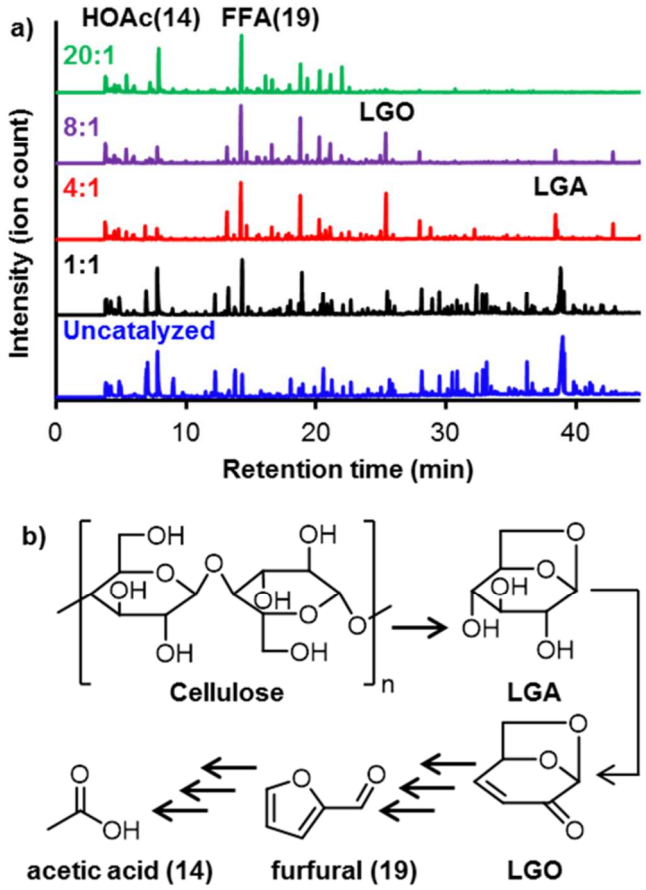

Figure 4: (a) Pyrograms of biomass in the presence of indicated $Ni_2P@Mo_2C$(1.89) catalyst:biomass weight ratios. Peak heights are normalized to the intensity of the tallest peak in each spectrum. b) Possible reaction pathway for cellulose pyrolysis to levoglucosan and subsequent reaction products.

Deconstruction of hemicellulose is expected to produce a similar family of compounds as cellulose, albeit with some variations. They are both composed of sugar monomers with cellulose being a linear homopolymer of anhydrous glucose and hemicellulose a branched heteropolymer of many types of sugars.[40] Lignin is a complex aromatic polymer and the deconstruction fragments range from relatively simple phenols to phenolic oligomers with molecular weights in the thousands.[41] When the catalyst to biomass ratio is 20:1, phenol is the only lignin monomer above the threshold used for analysis, even though several lignin-derived molecules are detected with the py-GC/MS configuration and conditions employed in our investigation (Figure S5). Although we can detect molecules such as phenol, guaiacol, cresol, vinylguaiacol, syringol, and others when whole biomass is pyrolyzed in the presence of catalyst, their relative intensity is greatly decreased in comparison to the sugar-derived molecules(Figure S5c).

As bio-oil typically contains hundreds of compounds, lowering the number of condensable products using catalysts is desirable, as this affords a bio-oil amenable to further processing and upgrading.[41,42] However, an increase in the amount of CO_2 and acetic acid is less desirable, as these indicate the loss of valuable carbon atoms as non-condensable gas or an increase in bio-oil acidity. One of the tools that can be used to tune bio-oil composition is to use a composite catalyst such as $Ni_2P@Mo_2C$. When the phosphide to carbide molar ratio (P:C) was varied from 0.16 to 18.8 and CFP was performed using a 20:1 catalyst to analyte ratio, a total of 27 molecules (Figure S4) were detected by MS. Table S1 shows fraction of each component in the final product based on the contribution of each molecule to the total ion current (TIC).

The Mo_2C catalyst system afforded the fewest products (Table S1 and Figure S6-S7). The product slate of Mo_2C and low phosphide loaded composites is dominated by oxygenates, i.e.

carbon dioxide (1), acetaldehyde (2), methyl acetate (6) and acetic acid (14). Contribution from these oxygenates decreases gradually with increasing phosphide loading as is evident across Table S1. The dominant product at the optimal phosphide loading (P:C = 1.89) is furfural (19), with significant contributions from methyl furan (7), 5-methyl furfural (23), and acetyl furan (21). At the highest phosphide loading (P:C = 18.8), and for the unsupported phosphide (Ni_xP_y), the product slate is dominated by furans such as 2,5-dimethyl furan (13) in addition to furfurals and cyclic ketones. There is a gradual increase in furans, furfurals and cyclic ketones as the phosphide loading increases. These patterns are seen with very high consistency up to the optimum carbide-phosphide ratio (1.89), beyond which the deposited phosphide appears as a biphasic material and the distribution patterns for many products become inconsistent. The results demonstrate that modification of carbide surface via deposition of phosphide at various P:C can be used to tune the product slate and increase the proportion of desired product molecules with higher C:O ratio.

We attribute the tunability in the product slate to the presence of bimetallic interfacial sites formed via deposition of phosphide on carbide. Since XPS indicates intermetallic interaction akin to doped and alloyed bimetallic catalysts between the two transition metals,[18] we infer that unique bimetallic active sites are generated during hydrothermal deposition of phosphide on carbide. Further investigations are necessary to characterize the interfacial sites to determine possible bimetallic active sites in addition to those present in Mo_2C and Ni_2P. However, the product slate for the catalyst system consisting of a physical mixture of phosphide and carbide (mix) with the same molar Ni:Mo as in the optimum phosphide deposition catalyst (1.89) is demonstrably different to that of the optimum phosphide deposited catalyst. The physical

mixture shows higher degree of complexity and the product distribution does not match any of the composite catalysts (Table S1).

The unsupported phosphide (Ni_xP_y) and phosphide supported on MWCNT (MW) show almost identical distribution. The Ni_xP_y-catalyzed system includes 3-methylcyclopentene (8), 2-ethylfuran (12), and cyclopentanone (15), but these compounds are absent in the MW product slate. Similarly, the product slate for MW contains 5-methyl furfural (23), but this product is absent when Ni_xP_y is used. The rest of the compounds in the two systems show an almost identical distribution, unlike phosphide deposited carbide composite catalysts. Evidently, contribution to product slate tunability from interfacial sites between Ni_xP_y and MWCNT does not have the same consequence as interfacial sites formed by Ni_2P-Mo_2C interactions.

The distribution of products was analyzed based on the C:O ratio in each fraction, and is shown in Figure 5 (full representative pyrograms are shown in Figure S8-S18). As shown in Figure 5b, the increased deposition of phosphide on carbide increases the proportion of molecules with higher C:O. In addition, changing the carbide to phosphide ratio in the catalyst results in a product slate with varying compositions in each C:O fraction.

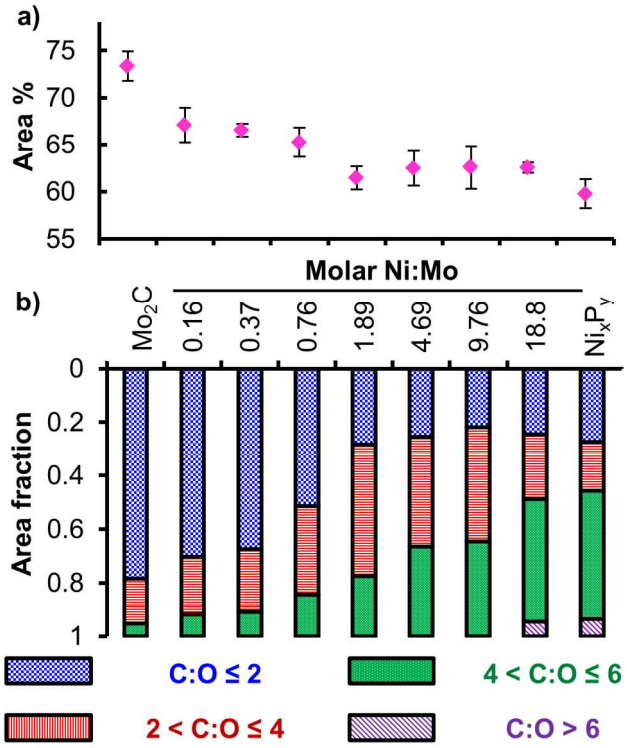

Figure 5: (a) Percent of the total area under the curve represented by the peaks above the threshold (10 % by height) from ex-situ catalytic fast pyrolysis of biomass at 450 °C and 20:1 catalyst to biomass ratios. The values are the average of four independent experiments and error bars represent the computed standard deviations. (b) Distribution based on carbon to oxygen atomic ratio of products above the threshold.

Such tunability in the composition of the product slate is afforded by synthetically tailoring the catalysts. The fraction distribution of the lowest phosphide-carbide ratio catalyst (0.16) resembles the system catalyzed by Mo_2C, and the highest ratio (18.8) resembles Ni_xP_y. In between the two extremes, while there is a general increase in the fractions with C:O≥2 with higher phosphide loading and gradual decrease in fractions with C:O≤2, there is also variability within the higher C:O fractions. Of particular note is the increase in the contribution of the second fraction (2<C:O≤4) which increases up to the optimum phosphide-carbide ratio and then

decreases. This effect can be attributed to the interfacial sites that are formed with increasing population until the optimum ratio.

Catalyst stability

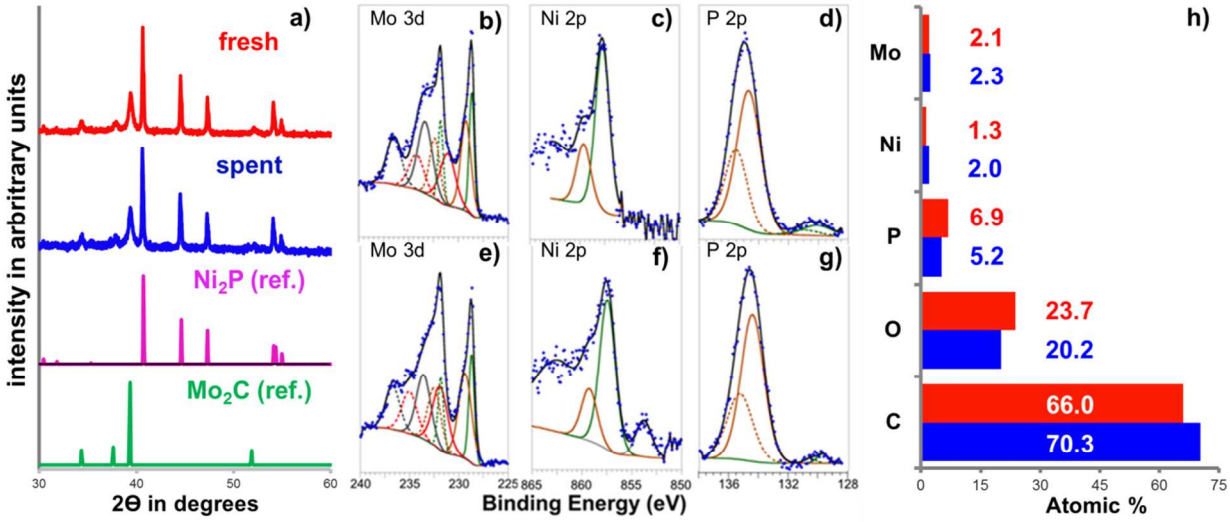

Figure 6: a) XRD plots for composite phosphide-carbide catalyst before (fresh) and after (spent) biomass upgrading. The composite catalyst is $Ni_2P@Mo_2C(1.89)$ and the catalyst to biomass ratio is 20:1 XPS spectra pre-catalysis corresponding to b) Mo 3d c) Ni 2p and d) P 2p. Post-catalysis XPS spectra corresponding to e) Mo 3d f) Ni 2p g) P 2p. Solid color-coded deconvolution lines in Mo 3d and P 2p spectra correspond to $d_{5/2}$ and $p_{3/2}$, respectively. Color matched dotted lines correspond to $d_{3/2}$ and $p_{½}$. h) Bar graph for atomic percent of the fresh (red) and spent (blue) catalyst surfaces determined via XPS.

XRD plots in Figure 6a show that the crystal structure of composite catalyst does not change significantly during VPU of biomass. However, comparison of XPS spectra of composite materials before and after catalysis (Figure 6, b-g) reveals an increase in metallic character of the catalyst surfaces after catalysis. This is exemplified by the abundance of peaks pertaining to

oxidized nickel species before catalysis (Table S2). After catalysis, a peak corresponding to the more reduced nickel phosphide (853.78 eV), which accounts for 15 % of the Ni 2p peak fraction, is evident.[43] Li and coworkers have shown previously that supported Ni_2P readily forms Ni^{2+} species in air,[44] and Okamoto and coworkers have noted an O-atom transfer from nickel to phosphorus upon heat treatment of nickel phosphide.[45] Our experimental data support these findings, as we note a decrease in oxidized nickel species with a concomitant increase in oxidized phosphorus species after catalysis. Atomic composition of the surfaces in Figure 6h also shows slight increase in atomic percentage of transition metals and reduction in atomic percentage of oxygen and phosphorus.

The EDS elemental maps in Figure S19 for as synthesized and post-VPU catalysts show analogous distribution of elements before and after catalysis. Absence of significant aggregation post-catalysis of any constituent element shows that the carbide-phosphide composite materials are stable during the reaction conditions employed during catalytic fast pyrolysis.

CONCLUSIONS

In summary, we have demonstrated that preparation of carbide and deposition of phosphide on carbide are both relatively simple methods that can be readily scaled up to pilot and industrial scale thermochemical conversion of biomass. The resulting carbide-phosphide interaction is critical in retaining monophasic phosphide material under annealing conditions at 500 °C in argon. We have further demonstrated the utility of the carbide-phosphide composites for the vapor-phase upgrading (VPU) of biomass. Composition of the VPU product can be tuned by changing the catalyst composition. VPU of CFP products using nickel phosphide and molybdenum carbide results in markedly different product slates. Metal carbide-phosphide

interfacial sites evidently provide a unique active site, unlike phosphide deposited on carbon. Composite materials thus can be used to engineer systems to produce targeted VPU products via CFP.

ASSOCIATED CONTENT

Supporting Information.

The following files are available free of charge.

Thermogravimetric analysis (TGA) plot of carbide-phosphide composite catalyst, full representative pyrograms with peaks above threshold marked with arrows in each pyrogram, table of contribution of each fraction to the TIC with statistical errors, XPS spectra deconvoluted area fractions corresponding to Figure 6b-g, and scanning electron micrographs of composite catalysts, EDX elemental maps and spectrum.

AUTHOR INFORMATION

Corresponding Author

*** E-mail: schmely@utk.edu and nlabbe@utk.edu**

Author Contributions

The manuscript was written through contributions of all authors. All authors have given approval to the final version of the manuscript.

Funding Sources

This project was supported by funds from the Southeastern Sun Grant Center and the US Department of Transportation, Research and Innovative Technology Administration DTO559-

07-G-00050. Additional support was provided by Logistics for Enhanced-Attribute Feedstocks (LEAF), a project funded by the Department of Energy, Office of Energy Efficiency and Renewable Energy (EERE), Award Number EE0006639. N.L and S.C.C. also acknowledge the Southeastern Partnership for Integrated Biomass Supply Systems (IBSS), which is supported by AFRI 2011-68005-30410 from USDA NIFA. XRD was performed at the Joint Institute for Advanced Materials (JIAM) using instruments that were procured via the DOE-Nuclear Energy University Program (DE-NE0000693).

ACKNOWLEDGMENT

The authors would like to thank Ms. Choo Hamilton at the Center for Renewable Carbon (CRC) for assistance with ICP-OES, and Dr. John R. Dunlap, Dr. Maulik Patel, and Mr. Graham S. Collier at Joint Institute for Advanced Materials (JIAM) for assistance with TEM, EDS, XRD, and TGA. We would also like to thank Dr. James R. McBride, Department of Chemistry at Vanderbilt University and Vanderbilt Institute of Nanoscale Science and Engineering, for assistance with TEM-EDS.

REFERENCES

(1) Robinson, A. M.; Hensley, J. E.; Medlin, J. W.: Bifunctional Catalysts for Upgrading of Biomass-Derived Oxygenates: A Review. *ACS Catal.* **2016**, *6*, 5026-5043.

(2) Ruddy, D. A.; Schaidle, J. A.; Ferrell Iii, J. R.; Wang, J.; Moens, L.; Hensley, J. E.: Recent advances in heterogeneous catalysts for bio-oil upgrading via "ex situ catalytic fast pyrolysis": catalyst development through the study of model compounds. *Green Chem.* **2014**, *16*, 454-490.

(3) Rinaldi, R.; Jastrzebski, R.; Clough, M. T.; Ralph, J.; Kennema, M.; Bruijnincx, P. C.; Weckhuysen, B. M.: Paving the Way for Lignin Valorisation: Recent Advances in Bioengineering, Biorefining and Catalysis. *Angew. Chem. Int. Ed. Engl.* **2016**, *55*, 8164-215.

(4) Zhao, H. Y.; Li, D.; Bui, P.; Oyama, S. T.: Hydrodeoxygenation of guaiacol as model compound for pyrolysis oil on transition metal phosphide hydroprocessing catalysts. *Appl. Catal. A* **2011**, *391*, 305-310.

(5) Bridgwater, A. V.: Review of fast pyrolysis of biomass and product upgrading. *Biomass Bioenerg.* **2012**, *38*, 68-94.

(6) Griffin, M. B.; Baddour, F. G.; Habas, S. E.; Ruddy, D. A.; Schaidle, J. A.: Evaluation of Silica-Supported Metal and Metal Phosphide Nanoparticle Catalysts for the Hydrodeoxygenation of Guaiacol Under Ex Situ Catalytic Fast Pyrolysis Conditions. *Top. Catal.* **2015**, *59*, 124-137.

(7) Habas, S. E.; Baddour, F. G.; Ruddy, D. A.; Nash, C. P.; Wang, J.; Pan, M.; Hensley, J. E.; Schaidle, J. A.: A Facile Molecular Precursor Route to Metal Phosphide Nanoparticles and Their Evaluation as Hydrodeoxygenation Catalysts. *Chem. Mater.* **2015**, *27*, 7580-7592.

(8) Ren, H.; Yu, W.; Salciccioli, M.; Chen, Y.; Huang, Y.; Xiong, K.; Vlachos, D. G.; Chen, J. G.: Selective hydrodeoxygenation of biomass-derived oxygenates to unsaturated hydrocarbons using molybdenum carbide catalysts. *ChemSusChem* **2013**, *6*, 798-801.

(9) Rensel, D. J.; Kim, J.; Bonita, Y.; Hicks, J. C.: Investigating the multifunctional nature of bimetallic FeMoP catalysts using dehydration and hydrogenolysis reactions. *Appl. Catal. A* **2016**, *524*, 85-93.

(10) Oyama, S.: Novel catalysts for advanced hydroprocessing: transition metal phosphides. *J. Catal.* **2003**, *216*, 343-352.

(11) Choi, J.-S.; Zacher, A. H.; Wang, H.; Olarte, M. V.; Armstrong, B. L.; Meyer, H. M.; Soykal, I. I.; Schwartz, V.: Molybdenum Carbides, Active andIn SituRegenerable Catalysts in Hydroprocessing of Fast Pyrolysis Bio-Oil. *Energ. Fuel.* **2016**, *30*, 5016-5026.

(12) Regmi, Y. N.; Wan, C.; Duffee, K. D.; Leonard, B. M.: Nanocrystalline Mo2C as a Bifunctional Water Splitting Electrocatalyst. *ChemCatChem* **2015**, *7*, 3911-3915.

(13) Han, J.; Duan, J.; Chen, P.; Lou, H.; Zheng, X.; Hong, H.: Nanostructured molybdenum carbides supported on carbon nanotubes as efficient catalysts for one-step hydrodeoxygenation and isomerization of vegetable oils. *Green Chem.* **2011**, *13*, 2561.

(14) Kelly, T. G.; Chen, J. G.: Controlling C–O, C–C and C–H bond scission for deoxygenation, reforming, and dehydrogenation of ethanol using metal-modified molybdenum carbide surfaces. *Green Chem.* **2014**, *16*, 777-784.

(15) Bej, S. K.; Bennett, C. A.; Thompson, L. T.: Acid and base characteristics of molybdenum carbide catalysts. *Appl. Catal. A* **2003**, *250*, 197-208.

(16) Sullivan, M. M.; Bhan, A.: Acetone Hydrodeoxygenation over Bifunctional Metallic–Acidic Molybdenum Carbide Catalysts. *ACS Catal.* **2016**, *6*, 1145-1152.

(17) Chen, C.-J.; Lee, W.-S.; Bhan, A.: Mo2C catalyzed vapor phase hydrodeoxygenation of lignin-derived phenolic compound mixtures to aromatics under ambient pressure. *Appl. Catal. A* **2016**, *510*, 42-48.

(18) Regmi, Y. N.; Roy, A.; Goenaga, G. A.; McBride, J. R.; Rogers, B. R.; Zawodzinski, T. A.; Labbé, N.; Chmely, S. C.: Electrocatalytic Activity and Stability Enhancement through Preferential Deposition of Phosphide on Carbide. *ChemCatChem* **2017**, *9*, 1054-1061.

(19) Mortensen, P. M.; Grunwaldt, J.-D.; Jensen, P. A.; Jensen, A. D.: Screening of Catalysts for Hydrodeoxygenation of Phenol as a Model Compound for Bio-oil. *ACS Catal.* **2013**, *3*, 1774-1785.

(20) Ardiyanti, A. R.; Khromova, S. A.; Venderbosch, R. H.; Yakovlev, V. A.; Melián-Cabrera, I. V.; Heeres, H. J.: Catalytic hydrotreatment of fast pyrolysis oil using bimetallic Ni–Cu catalysts on various supports. *Appl. Catal. A* **2012**, *449*, 121-130.

(21) Koike, N.; Hosokai, S.; Takagaki, A.; Nishimura, S.; Kikuchi, R.; Ebitani, K.; Suzuki, Y.; Oyama, S. T.: Upgrading of pyrolysis bio-oil using nickel phosphide catalysts. *J. Catal.* **2016**, *333*, 115-126.

(22) Wu, S.-K.; Lai, P.-C.; Lin, Y.-C.; Wan, H.-P.; Lee, H.-T.; Chang, Y.-H.: Atmospheric Hydrodeoxygenation of Guaiacol over Alumina-, Zirconia-, and Silica-Supported Nickel Phosphide Catalysts. *ACS Sustainable Chem. Eng.* **2013**, *1*, 349-358.

(23) Regmi, Y. N.; Leonard, B. M.: General Synthesis Method for Bimetallic Carbides of Group VIIIA First Row Transition Metals with Molybdenum and Tungsten. *Chem. Mater.* **2014**, *26*, 2609-2616.

(24) Deng, Y.; Zhou, Y.; Yao, Y.; Wang, J.: Facile synthesis of nanosized nickel phosphides with controllable phase and morphology. *New J. Chem.* **2013**, *37*, 4083.

(25) Moulder J. F., S. W. F. S. P. E., Bomben K. D. : *Handbook of X-Ray Photoelectron Spectroscopy*; Perkin-Elmer Corp: Eden Prairie, MN, 1995.

(26) Lindsey, K.; Johnson, A.; Kim, P.; Jackson, S.; Labbé, N.: Monitoring switchgrass composition to optimize harvesting periods for bioenergy and value-added products. *Biomass Bioenerg.* **2013**, *56*, 29-37.

(27) Kim, P.; Rials, T. G.; Labbé, N.; Chmely, S. C.: Screening of Mixed-Metal Oxide Species for Catalytic Ex Situ Vapor-Phase Deoxygenation of Cellulose by py-GC/MS Coupled with Multivariate Analysis. *Energ. Fuel.* **2016**, *30*, 3167-3174.

(28) Zhao, Q.; Han, Y.; Huang, X.; Dai, J.; Tian, J.; Zhu, Z.; Yue, L.: Hydrothermal synthesis of Ni2P nanoparticle and its hydrodesulfurization of dibenzothiophene. *J. Nanopart. Res.* **2017**, *19*.

(29) Tang, C.; Wang, W.; Sun, A.; Qi, C.; Zhang, D.; Wu, Z.; Wang, D.: Sulfur-Decorated Molybdenum Carbide Catalysts for Enhanced Hydrogen Evolution. *ACS Catal.* **2015**, *5*, 6956-6963.

(30) de Largy, B.; Finch, A.; Gardner, P. J.; Kell, N.: The retarded sublimation of red phosphorus. *J. Chem. Soc., Faraday* **1983**, *79*, 383.

(31) Zhang, Y.; Rui, X.; Tang, Y.; Liu, Y.; Wei, J.; Chen, S.; Leow, W. R.; Li, W.; Liu, Y.; Deng, J.; Ma, B.; Yan, Q.; Chen, X.: Wet-Chemical Processing of Phosphorus Composite Nanosheets for High-Rate and High-Capacity Lithium-Ion Batteries. *Adv. Energy Mat.* **2016**, *6*, 1502409.

(32) Kawasaki, S.; Matsuoka, Y.; Yokomae, T.; Nojima, Y.; Okino, F.; Touhara, H.; Kataura, H.: XRD and TEM study of high pressure treated single-walled carbon nanotubes and C60-peapods. *Carbon* **2005**, *43*, 37-45.

(33) Laursen, A. B.; Patraju, K. R.; Whitaker, M. J.; Retuerto, M.; Sarkar, T.; Yao, N.; Ramanujachary, K. V.; Greenblatt, M.; Dismukes, G. C.: Nanocrystalline Ni5P4: a hydrogen evolution electrocatalyst of exceptional efficiency in both alkaline and acidic media. *Energy Environ. Sci.* **2015**, *8*, 1027-1034.

(34) Lee, W.-S.; Kumar, A.; Wang, Z.; Bhan, A.: Chemical Titration and Transient Kinetic Studies of Site Requirements in Mo2C-Catalyzed Vapor Phase Anisole Hydrodeoxygenation. *ACS Catal.* **2015**, *5*, 4104-4114.

(35) Li, Y.; Zhao, C.: Iron-Doped Nickel Phosphate as Synergistic Electrocatalyst for Water Oxidation. *Chem. Mater.* **2016**, *28*, 5659-5666.

(36) Abu, I.; Smith, K.: The effect of cobalt addition to bulk MoP and Ni2P catalysts for the hydrodesulfurization of 4,6-dimethyldibenzothiophene. *J. Catal.* **2006**, *241*, 356-366.

(37) Balat, M.: Mechanisms of Thermochemical Biomass Conversion Processes. Part 1: Reactions of Pyrolysis. *Energ. Source A* **2008**, *30*, 620-635.

(38) Zhou, X.; Nolte, M. W.; Mayes, H. B.; Shanks, B. H.; Broadbelt, L. J.: Experimental and Mechanistic Modeling of Fast Pyrolysis of Neat Glucose-Based Carbohydrates. 1. Experiments and Development of a Detailed Mechanistic Model. *Ind. Eng. Chem. Res.* **2014**, *53*, 13274-13289.

(39) Lin, Y.-C.; Cho, J.; Tompsett, G. A.; Westmoreland, P. R.; Huber, G. W.: Kinetics and Mechanism of Cellulose Pyrolysis. *J. Phys. Chem. C* **2009**, *113*, 20097-20107.

(40) Alonso, D. M.; Wettstein, S. G.; Dumesic, J. A.: Bimetallic catalysts for upgrading of biomass to fuels and chemicals. *Chem. Soc. Rev.* **2012**, *41*, 8075-98.

(41) Oasmaa, A.; Czernik, S.: Fuel Oil Quality of Biomass Pyrolysis OilsState of the Art for the End Users. *Energ. Fuel.* **1999**, *13*, 914-921.

(42) Oasmaa, A.; Kuoppala, E.; Solantausta, Y.: Fast Pyrolysis of Forestry Residue. 2. Physicochemical Composition of Product Liquid. *Energ. Fuel.* **2003**, *17*, 433-443.

(43) Grosvenor, A. P.; Biesinger, M. C.; Smart, R. S.; McIntyre, N. S.: New interpretations of XPS spectra of nickel metal and oxides. *Surf. Sci.* **2006**, *600*, 1771-1779.

(44) Li, K. L.; Wang, R. J.; Chen, J. X.: Hydrodeoxygenation of Anisole over Silica-Supported Ni2P, MoP, and NiMoP Catalysts. *Energ. Fuel.* **2011**, *25*, 854-863.

(45) Okamoto, Y.; Nitta, Y.; Imanaka, T.; Teranishi, S.: Surface Characterization of Nickel Boride and Nickel Phosphide Catalysts by X-Ray Photoelectron-Spectroscopy. *J. Chem. Soc., Faraday* **1979**, *75*, 2027-2039.

Table of Contents

Scalable and Tunable Carbide-Phosphide Composite Catalyst System for the Thermochemical Conversion of Biomass

Yagya N. Regmi, B. R. Rogers, Nicole Labbé and Stephen C. Chmely

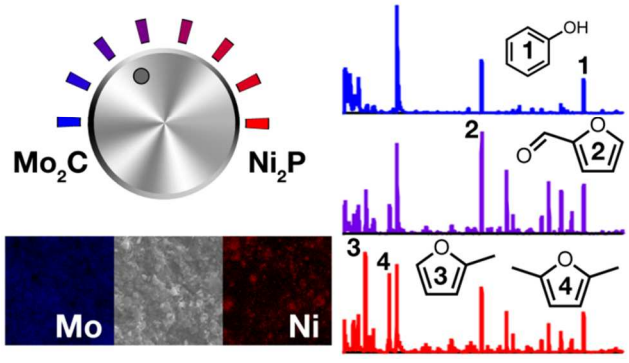

Variation in the molar ratio of nickel phosphide to molybdenum carbide in the hydrothermally prepared carbide-phosphide composite catalyst results in a tunable vapor products slate from catalytic fast pyrolysis of biomass.